

# Probabilistic bearing capacity of strip footing on reinforced anisotropic soil slope

Koushik Halder<sup>a</sup> and Debarghya Chakraborty\*

Department of Civil Engineering, Indian Institute of Technology Kharagpur, Kharagpur 721302, India

(Received April 26, 2019, Revised August 17, 2020, Accepted August 26, 2020)

**Abstract.** The probabilistic bearing capacity of a strip footing placed on the edge of a purely cohesive reinforced soil slope is computed by combining lower bound finite element limit analysis technique with random field method and Monte Carlo simulation technique. To simulate actual field condition, anisotropic random field model of undrained soil shear strength is generated by using the Cholesky-Decomposition method. With the inclusion of a single layer of reinforcement, dimensionless bearing capacity factor,  $N$  always increases in both deterministic and probabilistic analysis. As the coefficient of variation of the undrained soil shear strength increases, the mean  $N$  value in both unreinforced and reinforced slopes reduces for particular values of correlation length in horizontal and vertical directions. For smaller correlation lengths, the mean  $N$  value of unreinforced and reinforced slopes is always lower than the deterministic solutions. However, with the increment in the correlation lengths, this difference reduces and at a higher correlation length, both the deterministic and probabilistic mean values become almost equal. Providing reinforcement under footing subjected to eccentric load is found to be an efficient solution. However, both the deterministic and probabilistic bearing capacity for unreinforced and reinforced slopes reduces with the consideration of loading eccentricity.

**Keywords:** strip footing; reinforced slope; vertical and eccentric load; lower bound limit analysis; anisotropic random model; monte-carlo simulation

## 1. Introduction

Over the last few decades, polymeric geosynthetics are used to improve both the stability and settlement characteristics of various geotechnical structures. The effectiveness of polymeric geosynthetics increases significantly for the structures such as foundations for buildings, bridge abutments, electrical transmission towers, and hanging cable cars constructed on the sloping ground or hilly terrain. Utilization of reinforcement enhances both the load carrying capacity of the foundation as well as the stability of the slope (Ghanbari *et al.* 2013). Prior experimental investigations (Selvadurai and Gnanendran 1989, Lee and Manjunath 2000, Yoo 2001, Turker *et al.* 2014, Keskin and Laman 2014, Zheng *et al.* 2019) as well as numerical analyses (Huang and Tatsuoka 1994; Zheng and Fox 2017, Zheng *et al.* 2018, Luo and Bathurst 2018, Halder and Chakraborty 2018, 2019a, b) also confirmed the usefulness of reinforcement layers in increasing the load-bearing capacity of footing placed on the soil slopes. In most of the prior research works, reinforcement was mainly utilized in the cohesionless soil. Noorzad and Mirmoradi (2010), Vahedifard *et al.* (2014), Wang *et al.* (2011), Abd and Utili (2017), and Chen *et al.* (2018) investigated the

effectiveness of reinforcements in cohesive soil and found that planar reinforcements like geotextile and geogrid can also increase the strength of cohesive soil. However, no studies were found in the literature that investigates the effect of reinforcement layer on the bearing capacity of a strip foundation placed on top of a clayey soil slope. In addition to that, super structure load can be eccentric due to structural asymmetry or architectural point of view. Previously conducted studies did not include that possibility of eccentric loading also.

As mentioned above, many researchers estimated the bearing capacity of a strip foundation resting on top of a reinforced soil slope but except Luo and Bathurst (2018), in all of the prior mentioned numerical studies, soil properties were considered deterministic. However, in reality, soil parameters vary significantly within a minimal distance in both horizontal as well as vertical directions (Phoon and Kulhawy 1999a, b). Thus, the assumption of constant value of soil parameters throughout the domain not only overestimates bearing capacity but also is unreliable as it fails to simulate the actual soil condition. For that reason, influence of soil spatial variability needs to be considered in the numerical analysis to make it more rational. The effect of spatial variability of soil parameters on the stability and settlement of various geotechnical structures were studied in the past by many researchers (Griffiths *et al.* 2002, Srivastava and Babu 2011, Yoo 2016, Lombardi *et al.* 2017, Pramanik *et al.* 2019, Halder and Chakraborty 2019c, 2020). In contrast, only some researchers (Luo and Bathurst 2017, 2018, Brahmi *et al.* 2018) considered the influence of spatial variability of soil parameters and estimated the

\*Corresponding author, Ph.D.

E-mail: [debarghya@civil.iitkgp.ac.in](mailto:debarghya@civil.iitkgp.ac.in)

<sup>a</sup>Ph.D.

E-mail: [koushikhalder@iitkgp.ac.in](mailto:koushikhalder@iitkgp.ac.in)

bearing capacity of a strip footing situated on the soil slope. Brahmī *et al.* (2018) modelled soil shear strength of cohesive soil as an isotropic random field. The assumption of modelling soil shear strength as an isotropic random field fails to reciprocate the actual soil heterogeneity, which leads to an erroneous result. Luo and Bathurst (2018) carried out probabilistic analysis of a large-scale reinforced cohesionless embankment subjected to strip loading. It is to be mentioned here that Luo and Bathurst (2018) considered a single set of values of the coefficient of variation of soil friction angle ( $CoV_\phi$ ), spatial correlation length in both horizontal ( $L_x$ ) and vertical ( $L_y$ ) directions which makes it case specific. According to the authors' knowledge, until now no probabilistic studies are carried out for the calculation of the bearing capacity of a strip footing placed on the reinforced cohesive soil slope with the consideration of anisotropic random field model and eccentric loading.

The first aspect of the present study is to compute the deterministic bearing capacity of the strip footing placed on the edge of a reinforced purely cohesive soil ( $\phi = 0^\circ$ ) slope and subjected to both vertical and eccentric loading. The second aspect of the present study is to incorporate the influence of clay anisotropy through random field modelling and compute the probabilistic bearing capacity of the strip footing. The lower bound finite element limit analysis method with second-order cone programming (SOCP) is used to carry out all the numerical analyses. The Monte-Carlo simulation technique is utilized to obtain the probabilistic outcomes. A series of deterministic analysis are performed by varying other parameters such as (i) slope angle ( $\beta$ ), (ii) loading eccentricity ( $e/B$ ), and (iii) embedment depth of reinforcement layer from the footing base ( $d/B$ ). The effectiveness of reinforcement in the deterministic analysis is expressed in terms of  $\eta$ , which is the ratio of ultimate collapse load of reinforced ( $Q_{u-r}$ ) and unreinforced ( $Q_{u-ur}$ ) soil slopes. Critical depth of reinforcement ( $d_{cr}/B$ ) corresponding to maximum efficiency factor ( $\eta_{max-det}$ ) is obtained for each value of  $\beta$ . Reinforcement layer is always kept at the optimum position for all probabilistic analyses. Undrained shear strength of soil ( $c$ ) is considered as a random variable. In addition to the parameters considered in the deterministic analyses, the influence of other parameters such as (i) coefficient of variation of the undrained shear strength of soil ( $CoV_c$ ), (ii) spatial correlation length in both horizontal ( $L_x$ ) and vertical ( $L_y$ ) directions are studied in probabilistic analyses. Footing remains to be at the slope edge in all numerical analyses to simulate the most vulnerable case as discussed in Halder *et al.* (2019). Probabilistic bearing capacity are presented in terms of design charts for various sets of  $CoV_c$ ,  $L_x$ , and  $L_y$ . Practising engineers are supposed to be benefited by using the design charts. Failure patterns of both unreinforced and reinforced soil slopes are obtained, in deterministic and probabilistic analyses.

## 2. Problem definition

A rigid, rough, and surface strip footing of width  $B$  as shown in Fig. 1(a) is situated at the edge of a reinforced purely cohesive soil slope with slope angle of  $\beta$ . Mean

value of undrained shear strength ( $c$ ) is taken as 20 kN/m<sup>2</sup>. A compressive load of  $Q_u$  is acting (i) at the centre of the footing ( $e/B = 0$ ) as well as (ii) at a distance of  $e/B = 0.5$  from slope edge. A reinforcement layer is laid throughout the length of the domain at a variable distance of  $d$ , measured from the base of the footing. The objective of the present study is to compute the lower bound deterministic as well as probabilistic bearing capacity of a strip footing. Following Yang *et al.* (2019 and 2020), dimensionless bearing capacity factor ( $N$ ) of a strip footing is determined as  $N = Q_u/cB$ . At the time of calculating  $N (= Q_{u-ur}/cB)$  for unreinforced slope,  $Q_{u-ur}$  is the corresponding collapse load of unreinforced slope. Similarly, for reinforced slope,  $Q_{u-r}$  is the corresponding collapse load based on which  $N (= Q_{u-r}/cB)$  is determined.

Failure in soil mass is assumed to occur by following the Mohr-Coulomb constitutive model. The associated flow rule is applied over the whole soil domain. Present study incorporates the influence of reinforcement by allowing shear stresses to be discontinuous and normal stresses to be continuous over the reinforcement position as proposed by Chakraborty and Kumar (2014). Bonding between reinforcement and soil is assumed entirely rough. The tensile strength of the reinforcement is considered very high so that no tearing of reinforcement is possible. Failure occurs only by shear between reinforcement and soil mass.

## 3. Boundary conditions and finite element mesh

As there is no overburden, normal ( $\sigma_x$  and  $\sigma_y$ ) and shear ( $\tau_{xy}$ ) stresses are zero along the boundary edge GH. The line HI denotes footing position. Footing-soil roughness condition is imposed with the help of the equation  $|\tau_{xy}| \leq c$ .

The values of  $\sigma_x$ ,  $\sigma_y$ , and  $\tau_{xy}$  are also kept equal to zero along slope edge IJ and vertical edge JE. Length, and depth of the problem domain in horizontal ( $L_H$ ) and vertical ( $L_V$ ) directions are sufficiently large to get unaffected by the failure surface. The expansion or reduction of the problem area should not affect the magnitude of collapse load. It is also ensured that the magnitudes of  $L_H$  and  $L_V$  should always be greater than the values of  $L_x$  and  $L_y$ . Two types of problem domain are selected depending upon the magnitude of  $L_x$  and  $L_y$ . The values of  $L_H$  and  $L_V$  are fixed as  $6.26B$  and  $6.55B$  for all the analyses where  $L_x$  and  $L_y$  values vary between  $0.25B$  and  $10B$ . For higher values of  $L_x$  and  $L_y$  ( $20B$  to  $60B$ ), the domain is extended up to  $75.98B$  and  $73.32B$  in the horizontal and vertical directions, respectively.

Two finite element meshes are used in the present study depending upon the values of  $L_x$  and  $L_y$ . Figs. 1(b) and 1(c) show typical finite element meshes obtained after discretizing a slope domain of  $\beta = 20^\circ$  by three noded triangular elements. Relatively finer mesh (refer: Fig. 1(b)) is used for  $L_x$  and  $L_y$  values between  $0.25B$  and  $10B$ . On the other hand, relatively coarser mesh (refer: Fig. 1(c)) is used for  $L_x$  and  $L_y$  values between  $20B$  and  $60B$ . However, in both the cases, mesh density is more near the footing region and it becomes less near the boundary sides. The notations  $N_d$ ,  $E$ ,  $D_c$ , and  $N_i$  in Figs. 1(b) and 1(c) express the total number of nodes, elements, discontinuities, and nodes

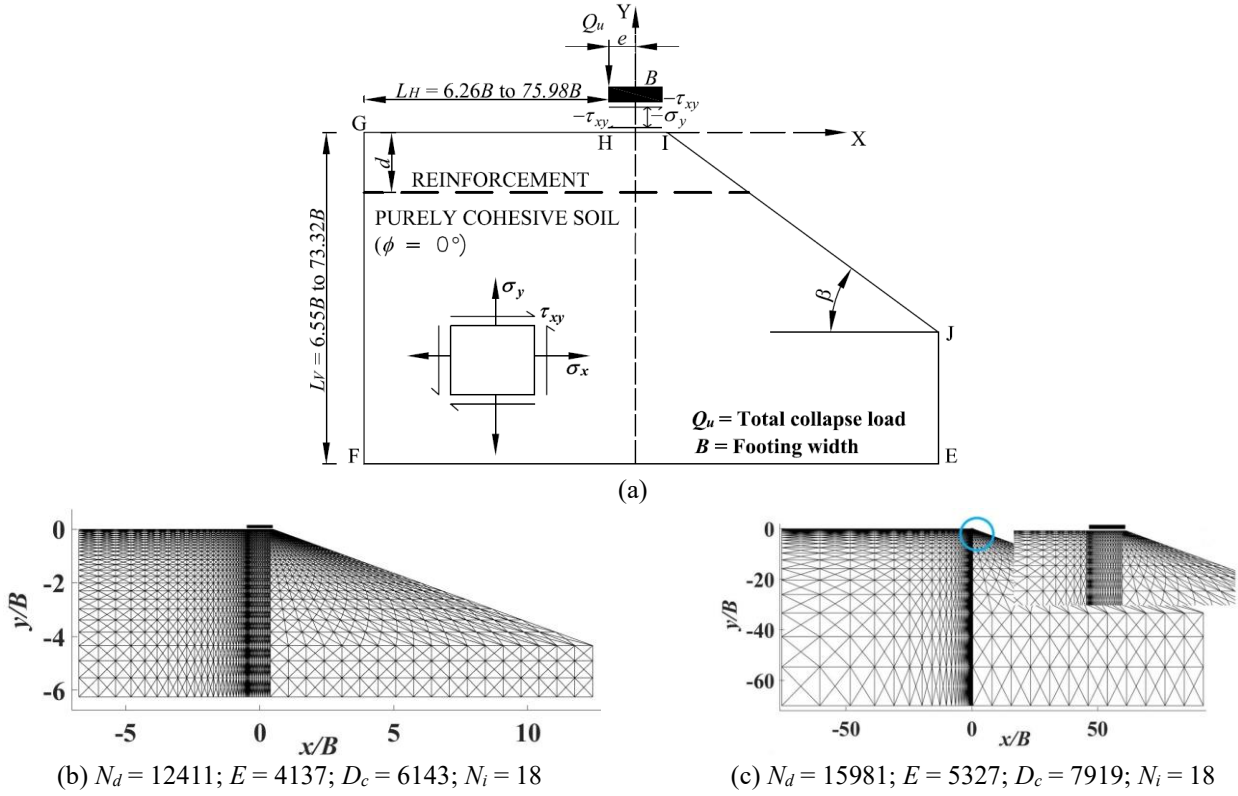


Fig. 1 (a) Problem domain and various stress boundary conditions; finite element mesh used in the study for  $\beta = 20^\circ$ ,  $c = 20$  kN/m<sup>2</sup> with (b)  $L_x/B = L_y/B = 0.25$  and (c)  $L_x/B = L_y/B = 40$

representing footing-soil interface, respectively. Fig. 1(c) also shows the zoomed portion of the finite element mesh near the footing.

## 4. Methodology

### 4.1 Lower bound finite element limit analysis

As aim of the present study is to predict the lower bound bearing capacity of the strip footing, the plane strain lower bound finite element limit analysis formulation of Sloan (1988) is employed. Second order conic optimization technique proposed by Makrodimopoulos and Martin (2006) is used to carry out conic optimization. Three noded triangular element as illustrated in Fig. 2(a) discretizes the problem domain in the two-dimensional object space ( $X$ - $Y$ ). The nodal stresses; normal stresses in the  $X$  and  $Y$  directions ( $\sigma_x$  and  $\sigma_y$ ) and shear stress ( $\tau_{xy}$ ) are the basic unknowns.

Variation of stresses are expressed in Eq. (1).

$$\sigma_x = \sum_{i=1}^3 N_{si} \sigma_{x,i}, \quad \sigma_y = \sum_{i=1}^3 N_{si} \sigma_{y,i}, \quad \tau_{xy} = \sum_{i=1}^3 N_{si} \tau_{xy,i} \quad i = 1, 2, \dots, N_d \quad (1)$$

In the above Eq. (1), nodal stresses associated with the  $i^{\text{th}}$  node are  $\sigma_{x,i}$ ,  $\sigma_{y,i}$ , and  $\tau_{xy,i}$ . Linear shape function associated with the  $i^{\text{th}}$  node is  $N_{si}$ . Various equality and inequality constraints generated during optimization are discussed briefly below. Details can be found in Sloan (1988) and Tang *et al.* (2014).

#### 4.1.1 Element equilibrium conditions

Static equilibrium conditions (Refer: Eq. (2)) are employed throughout the problem domain.

$$\frac{\partial \sigma_x}{\partial x} + \frac{\partial \tau_{xy}}{\partial y} = 0 \quad \text{and} \quad \frac{\partial \sigma_y}{\partial y} + \frac{\partial \tau_{xy}}{\partial x} = \gamma \quad (2)$$

Here,  $\gamma = \text{zero}$  for weightless soil condition. Because of that, two equality constraints are generated on nine nodal stresses (Refer: Eq. (3)).

$$[A^{el}]_{2 \times 9} \{ \sigma^{el} \}_{9 \times 1} = \{ b^{el} \}_{2 \times 1}; \quad (3)$$

$\{ \sigma^{el} \}^T = \{ \sigma_{x,1}^{el}, \sigma_{y,1}^{el}, \tau_{xy,1}^{el}, \sigma_{x,2}^{el}, \sigma_{y,2}^{el}, \tau_{xy,2}^{el}, \sigma_{x,3}^{el}, \sigma_{y,3}^{el}, \tau_{xy,3}^{el} \}$  is unknown stress vector and  $[A^{el}]_{2 \times 9}$ ,  $\{ b^{el} \}_{2 \times 1}$  are known matrices.

#### 4.1.2 Stress discontinuity conditions

Unlike the displacement based conventional finite element method, any node of an element is not shared between other adjacent elements in the lower bound finite element limit analysis technique. Nodes are distinct for all elements. Because of that, the interface between two surrounding triangles forms the edge of stress discontinuity as shown in Fig. 2(b). However, to make normal and shear stresses continuous over these edges, one needs to enforce discontinuity criterion over these edges. For an example, stress discontinuity conditions along the discontinuity edges formed by two adjacent triangles 'a' and 'b' will be as follows:

$$\begin{aligned} \sigma_{nm,1}^a = \sigma_{nm,2}^b; \quad \sigma_{nm,3}^a = \sigma_{nm,4}^b; \quad \tau_{sh,1}^a = \tau_{sh,2}^b; \\ \tau_{sh,3}^a = \tau_{sh,4}^b \end{aligned} \quad (4)$$

Magnitude of normal ( $\sigma_{nm}$ ) and shear stresses ( $\tau_{sh}$ ) can be obtained from Eq. (5).

$$\begin{aligned} \sigma_{nm} = \sin^2 \omega \sigma_x + \cos^2 \omega \sigma_y - \sin 2\omega \tau_{xy} \\ \tau_{sh} = -0.5 \sin 2\omega \sigma_x + 0.5 \sin 2\omega \sigma_y + \cos 2\omega \tau_{xy} \end{aligned} \quad (5)$$

Due to the implementation of stress discontinuity conditions (refer: Eq. (4)), four number of equality constraints are generated on twelve nodal stresses, which are expressed in Eq. (6).

$$[A^{ds}]_{4 \times 12} \{\sigma^{ds}\}_{12 \times 1} = \{b^{ds}\}_{4 \times 1} \quad (6)$$

where,

$$\begin{aligned} [A^{ds}]_{4 \times 12} &= \begin{bmatrix} S_d & -S_d & 0 & 0 \\ 0 & 0 & S_d & -S_d \end{bmatrix} \\ [S_d]_{2 \times 3} &= \begin{bmatrix} \sin^2 \omega & \cos^2 \omega & -\sin 2\omega \\ -0.5 \sin 2\omega & 0.5 \sin 2\omega & \cos 2\omega \end{bmatrix} \\ \{b^{ds}\}_{4 \times 1} &= \{0 \quad 0 \quad 0 \quad 0\} \end{aligned}$$

$$\{\sigma^{ds}\}_{12 \times 1} = \{\sigma_{x,1}^a \quad \sigma_{y,1}^a \quad \tau_{xy,1}^a \quad \sigma_{x,2}^b \quad \sigma_{y,2}^b \quad \tau_{xy,2}^b \quad \sigma_{x,3}^a \quad \sigma_{y,3}^a \quad \tau_{xy,3}^a \quad \sigma_{x,4}^b \quad \sigma_{y,4}^b \quad \tau_{xy,4}^b\}$$

In the above expressions, known quantities are  $[A^{ds}]$  and  $\{b^{ds}\}$ ; whereas, unknown is  $\{\sigma^{ds}\}$ . Angle of inclination between stress discontinuity edge and horizontal axis in anti-clockwise direction is  $\omega$ .

#### 4.1.3 Modification in stress discontinuity conditions for modelling of reinforcement

To incorporate the effect of including reinforcement layer, only the stress discontinuity conditions mentioned above need to be modified (Chakraborty and Kumar 2014). Following Chakraborty and Kumar (2014), the normal stress continuity on the discontinuous edges of the elements lying above and below the reinforcement layer is enforced; on the other hand, the shear stress continuity is relaxed as shown in Fig. 2(c). The modified stress discontinuity conditions are represented through Eq. (7). No explicit element is used to model the reinforcement layer. Hence, no input parameters related to reinforcement are required for the analysis. Reinforcement is assumed not to fail structurally in axial tension; however, a shear failure can occur along the interface between the soil and reinforcement. Interface between soil and reinforcement is assumed as fully bonded, i.e., the value of interface friction angle is same as that of soil friction angle.

$$\begin{aligned} \sigma_{nm,1}^a = \sigma_{nm,2}^b; \quad \sigma_{nm,3}^a = \sigma_{nm,4}^b; \quad \tau_{sh,1}^a \neq \tau_{sh,2}^b; \\ \tau_{sh,3}^a \neq \tau_{sh,4}^b \end{aligned} \quad (7)$$

#### 4.1.4 Stress boundary conditions

Stress boundary conditions employed over the boundary

edge of an element are shown in Fig. 2(d). In Fig. 2(d),  $\lambda$  denotes angle between boundary edge and horizontal axis in the anti-clockwise direction. Four equality constraints as expressed in Eq. (8) are generated on six nodal stresses due to the employment of stress boundary conditions.

$$[A^{sb}]_{4 \times 6} \{\sigma^{sb}\}_{6 \times 1} = \{b^{sb}\}_{4 \times 1} \quad (8)$$

where,

$$\begin{aligned} [A^{sb}] &= \begin{bmatrix} M_s & 0 \\ 0 & M_s \end{bmatrix}_{4 \times 6} \\ [M_s]_{2 \times 3} &= \begin{bmatrix} \sin^2 \lambda & \cos^2 \lambda & -\sin 2\lambda \\ -0.5 \sin 2\lambda & 0.5 \sin 2\lambda & \cos 2\lambda \end{bmatrix} \\ \{\sigma^{sb}\}^T &= \{\sigma_{x,1}^{sb} \quad \sigma_{y,1}^{sb} \quad \tau_{xy,1}^{sb} \quad \sigma_{x,2}^{sb} \quad \sigma_{y,2}^{sb} \quad \tau_{xy,2}^{sb}\}_{1 \times 6} \\ \{b^{sb}\}^T &= \{q_1 \quad t_1 \quad q_2 \quad t_2\}_{1 \times 4} \end{aligned}$$

Here,  $q_1$  and  $q_2$  are normal stresses acting on the boundary, and  $t_1$  and  $t_2$  are shear stresses acting along the boundary. Values of  $[A^{sb}]$  and  $\{b^{sb}\}$  are known; whereas,  $\{\sigma^{sb}\}$  is unknown.

#### 4.1.5 Yield criterion

Soil mass is assumed to follow the Mohr-Coulomb failure criterion as provided in Eq. (9).

$$F_{mc} = (\sigma_x - \sigma_y)^2 + (2\tau_{xy})^2 - 4c^2 \leq 0 \quad (9)$$

With the inclusion of second order cones at each node, the Mohr-Coulomb yield criterion becomes:

$$A_i^{SCP} \sigma_i^{SCP} + \xi_i = b_i^{SCP} \quad i = 1, 2, \dots, N_{nd} \quad (10)$$

where,

$$\begin{aligned} \sigma_i^{SCP} &= \{\sigma_{x,i}^{SCP} \quad \sigma_{y,i}^{SCP} \quad \tau_{xy,i}^{SCP}\}^T \\ \xi_i &= \{\xi_{1,i} \quad \xi_{2,i} \quad \xi_{3,i}\}^T; \quad b_i^{SCP} = \{2c, 0, 0\}^T \\ A_i^{SCP} &= \begin{bmatrix} 0 & 0 & 0 \\ -1 & 1 & 0 \\ 0 & 0 & -2 \end{bmatrix} \end{aligned}$$

$\xi_i$  is the conic vector.

#### 4.1.6 Objective function

The objective function (collapse load) for the present problem is obtained with the integration of the normal stresses associated with the nodes representing footing position (refer: Eq. (11)).

$$Q_u = \int_{L_s} \sigma^{OBJN} dl \quad (11)$$

In the above expression,  $Q_u$  is the magnitude of collapse load acting per unit width of the footing along the footing-soil interface of length  $L_s$ . The notations  $\sigma^{OBJN}$  and  $dl$  represent the average normal stress associated with the  $i^{\text{th}}$  element of footing-soil interface and the length of the  $i^{\text{th}}$

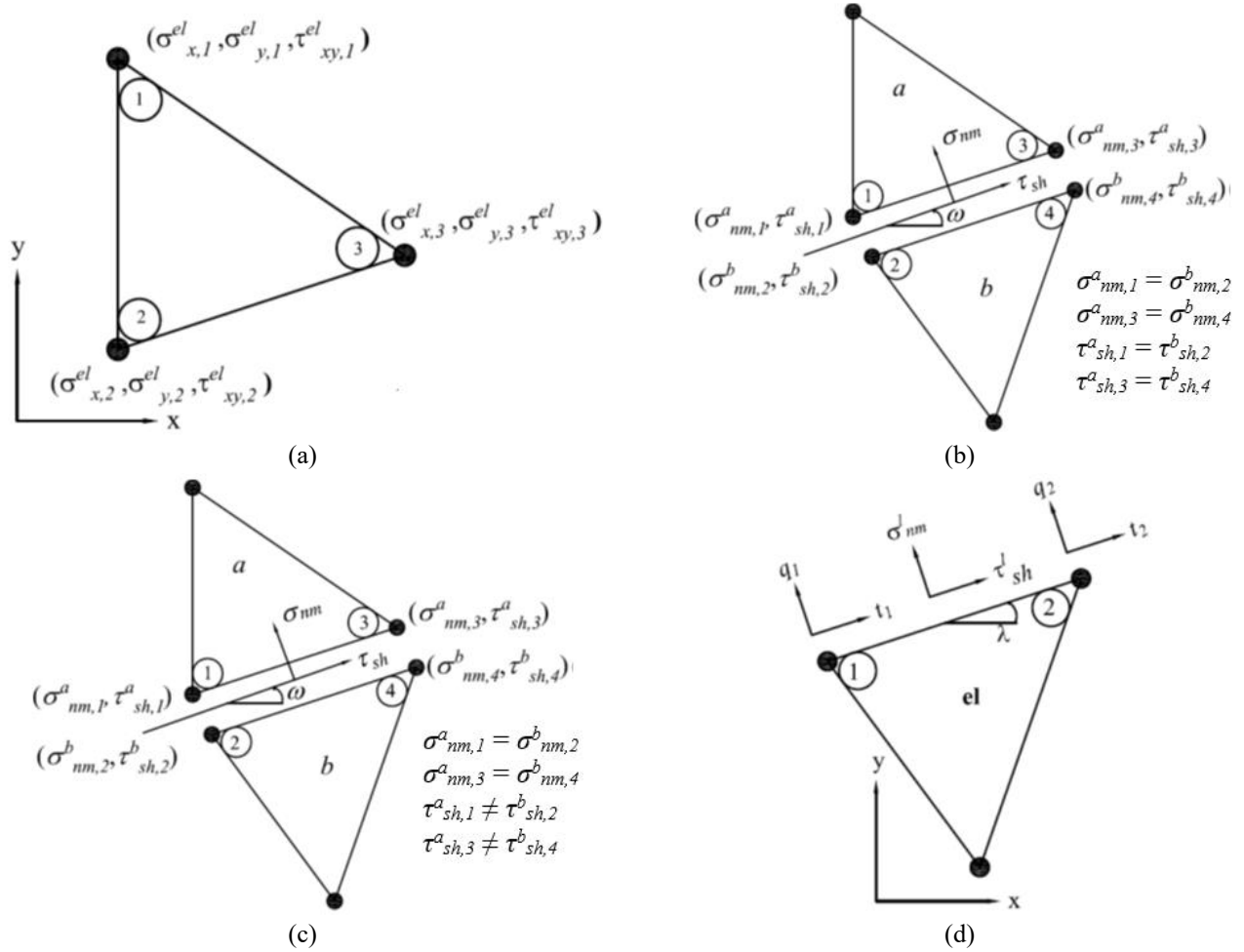


Fig. 2 (a) Three-noded linear stress triangle, (b) stress discontinuity conditions between two adjacent elements, (c) modified stress discontinuity conditions to incorporate reinforcement effect and (d) stress boundary equations applied over boundary edges

element.

#### 4.1.7 Final form of optimization

After the generation of all equality and conic constraints as mentioned in previous sections, these are assembled together to obtain global equality  $[A_{total}]$  matrices. The final form of the conic optimization scheme is outlined below.

$$\text{Maximize } \{g^T\} \{\sigma\} \quad (12)$$

subjected to,

$$[A_{total}] \{\sigma\} = \{b_{total}\}$$

whereas,

$$[A_{total}] = \begin{bmatrix} A_{eq} & 0 \\ A_{sb} & 0 \\ A_{ds} & 0 \\ A^{SCP} & I \end{bmatrix} \quad \text{and} \quad \{b_{total}\} = \begin{Bmatrix} b_{eq} \\ b_{sb} \\ b_{ds} \\ b^{SCP} \end{Bmatrix}$$

In the above expressions,  $\{g^T\}$  is the vector comprises of the objective function coefficients;  $\{\sigma\}$  is the global stress vector. A code is written in MATLAB to obtain the lower bound solution, whereas, an optimization toolbox MOSEK

is used to carry out conic optimization.

#### 4.2 Lower bound finite element limit analysis

An uncertainty associated with undrained shear strength (c) of purely cohesive soil is considered by modelling  $c$  as a random field. In order to avoid negative values of  $c$ ; the log-normal distribution is chosen. The anisotropic random field model of  $c$  is generated by using Cholesky-Decomposition technique. The auto-correlation function ( $\rho$ ) between values of  $c$  at two different points  $[(x_1, y_1) (x_2, y_2)]$  are obtained from Eq. (13).

$$\rho[(x_1, x_2)(y_1, y_2)] = \exp\left(-\frac{|x_1 - x_2|}{L_x} - \frac{|y_1 - y_2|}{L_y}\right) \quad (13)$$

Here,  $L_x$  and  $L_y$  are spatial correlation lengths in the horizontal and vertical directions.

#### 4.3 Combination of limit analysis and random field

After obtaining  $c$  value for each element from each Monte Carlo simulation, it is substituted in the following equation representing the Mohr-Coulomb failure criteria.

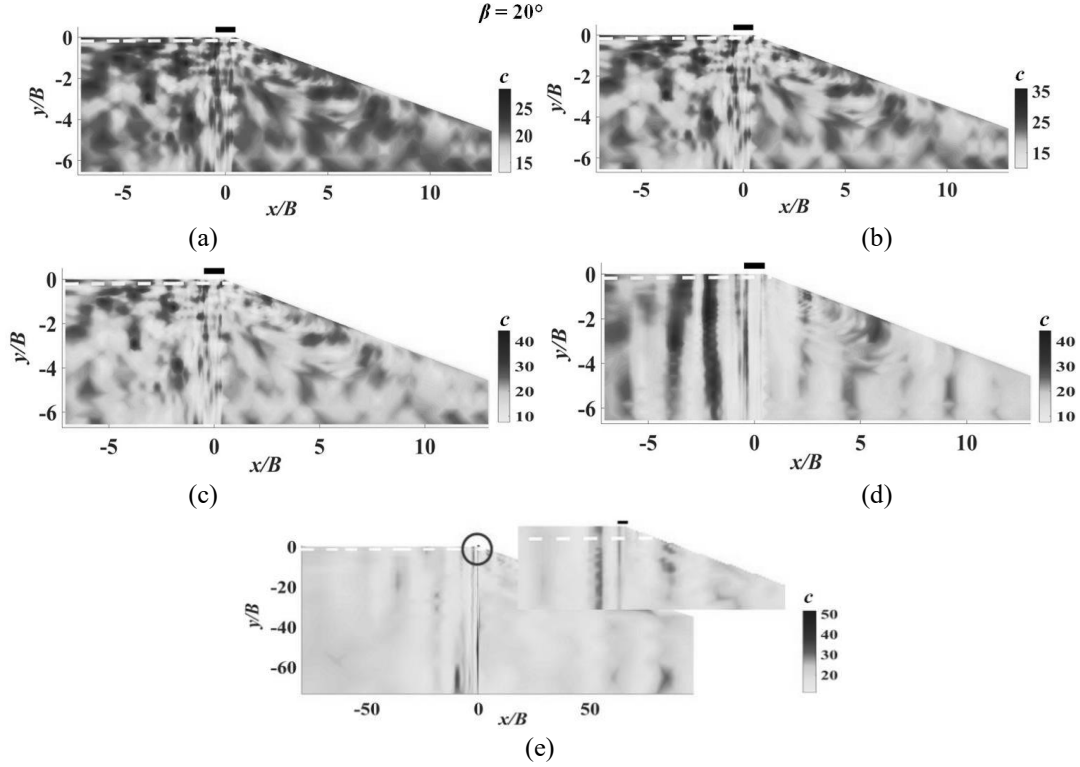


Fig. 3 Spatial distribution plot of undrained shear strength for reinforced slope of  $\beta = 20^\circ$  with (a);  $L_x = 0.25B$ ;  $L_y = 0.25B$ ,  $CoV_c = 15\%$ , (b)  $L_x = 0.25B$ ;  $L_y = 0.25B$ ;  $CoV_c = 25\%$ , (c)  $L_x = 0.25B$ ;  $L_y = 0.25B$ ;  $CoV_c = 35\%$ , (d)  $L_x = 0.25B$ ;  $L_y = 5B$ ;  $CoV_c = 35\%$  and (e)  $L_x = 0.25B$ ;  $L_y = 40B$ ;  $CoV_c = 35\%$

$$\sqrt{(\sigma_x - \sigma_y)^2 + (2\tau_{xy})^2} \leq 2c_j \quad (14)$$

In the above expression,  $c_j$  is the undrained shear strength of the  $j^{\text{th}}$  element where  $j$  changes from 1 to the total number of elements ( $E$ ). By using the modified Mohr-Coulomb failure criteria as per Eq. 9,  $N$  values for strip footing placed on the edge of unreinforced and reinforced slopes are obtained for each Monte-Carlo simulation technique.

#### 4.4 Failure probability

Failure probability of  $N$  associated with the strip footing placed on the reinforced slope is computed by using Eq. (15). In Eq. (15),  $FS$  denotes factor of safety considered by the design engineers. It is to be noted that during the design of foundations, design engineers use a  $FS$  value to obtain the safe bearing capacity by dividing the ultimate bearing capacity with  $FS$ .

$$p_{fNr} = p(N_i < N_{det} / FS) \quad (15)$$

whereas, the failure probability of efficiency factor ( $p_{fn}$ ) is computed by using Eq. (16) to study the influence of spatial variability of  $c$  on the effectiveness of reinforcement layer.

$$P_{fn} = \frac{n_F}{n_{Total}} \quad (16)$$

In the above expression, (i)  $n_F$  denotes number of simulations for which  $\eta_i$  values are less than the value of

$\eta_{det}$ , and (ii)  $n_{Total}$  is total number of simulations, i.e., 500 as Halder and Mahadevan (2000).

## 5. Results

For deterministic analysis, effectiveness of using reinforcement layer is presented in terms of the variation of the efficiency factor ( $\eta_{det}$ ) with the embedment depth of the reinforcement layer ( $d/B$ ) for two slope angles ( $\beta = 20^\circ$  and  $30^\circ$ ) and loading eccentricity ( $e/B = 0.0$  and  $0.5$ ). For the probabilistic studies of footing under vertical load, three values of  $CoV_c$  (15%, 25%, and 35%) are considered for two values of  $\beta = 20^\circ$  and  $30^\circ$ . The magnitude of  $L_x/B$  is varied as  $L_x/B = 0.25, 0.50, 1, 5, 10, 20, 40,$  and  $60$  and the magnitude of  $L_y/B$  is varied as  $L_y/B = 0.25, 0.50, 1, 2.5, 5, 10, 20, 40,$  and  $60$ . The values of  $L_x/B$  and  $L_y/B$  are considered as per Phoon and Kulhawy (1999a-b). In order to make the results non-dimensional, the magnitudes of  $L_x$  and  $L_y$  are chosen in terms of footing width ( $B$ ). In addition to that, the present study also aims to capture the effect of higher and lower spatial correlation length on the magnitude of bearing capacity factor  $N$  of a strip footing. For probabilistic analysis of strip footing subjected to eccentric loading, only a slope angle ( $\beta = 20^\circ$ ) and a single value of  $CoV_c$  (35%) is chosen.

### 5.1 Spatial distribution of undrained shear strength

Fig. 3 shows spatial distribution of undrained shear strength ( $c$ ) within a soil slope of  $\beta = 20^\circ$  for various

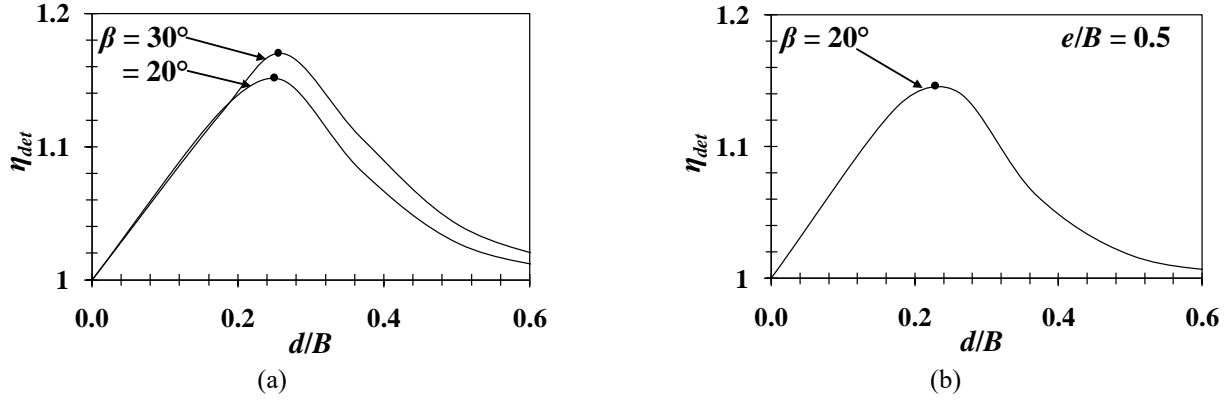


Fig. 4 Variation between  $\eta_{det}$  and  $d/B$  for  $\beta = 20^\circ$  and  $30^\circ$  in deterministic analysis and (b) Variation between  $\eta_{det}$  and  $d/B$  for  $\beta = 20^\circ$ ,  $e/B = 0.5$  in deterministic analysis

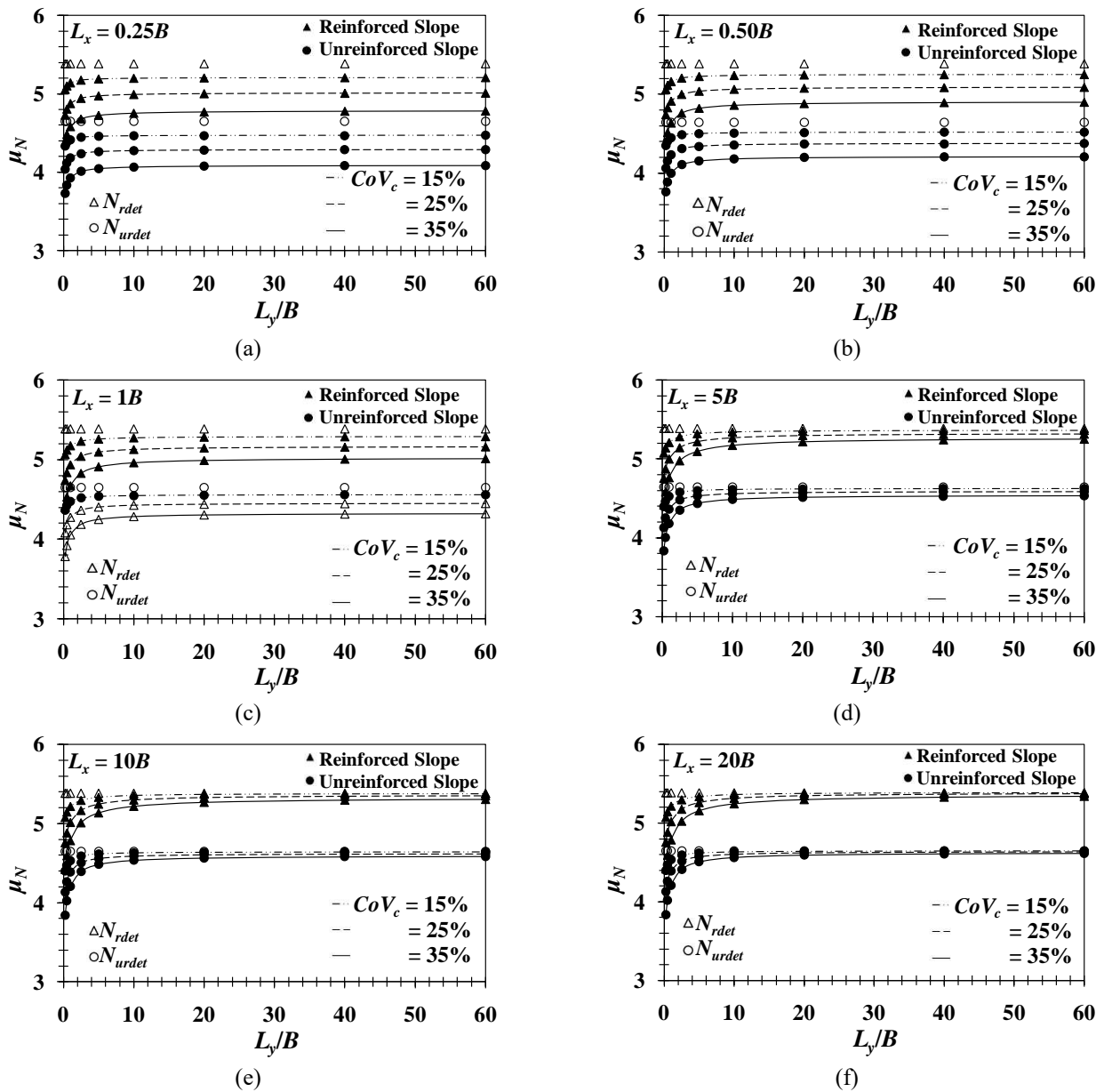


Fig. 5 Variation between  $\mu_N$ ,  $L_y/B$ , and  $CoV_c$  for unreinforced and reinforced slope of  $\beta = 20^\circ$  with  $L_x/B =$  (a) 0.25, (b) 0.50, (c) 1, (d) 5, (e) 10, (f) 20, (g) 40 and (h) 60

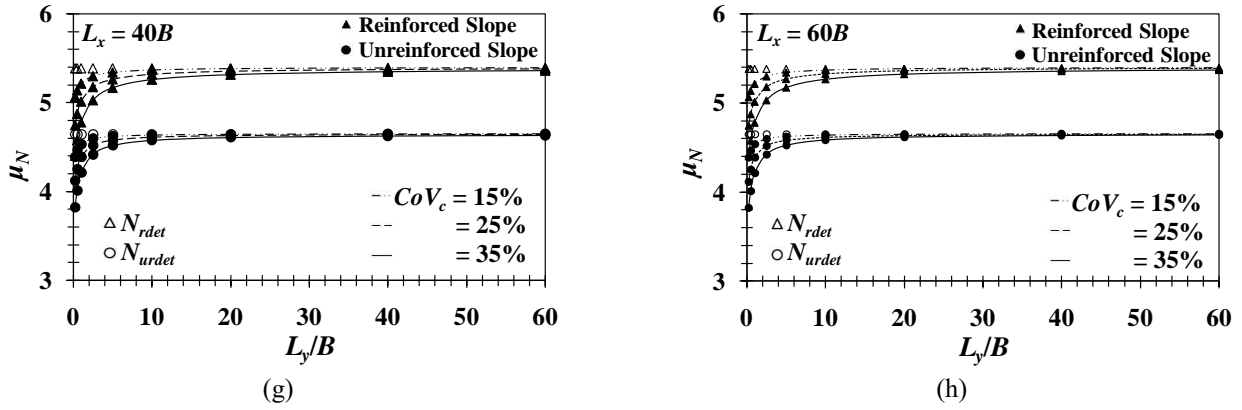


Fig. 5 Continued

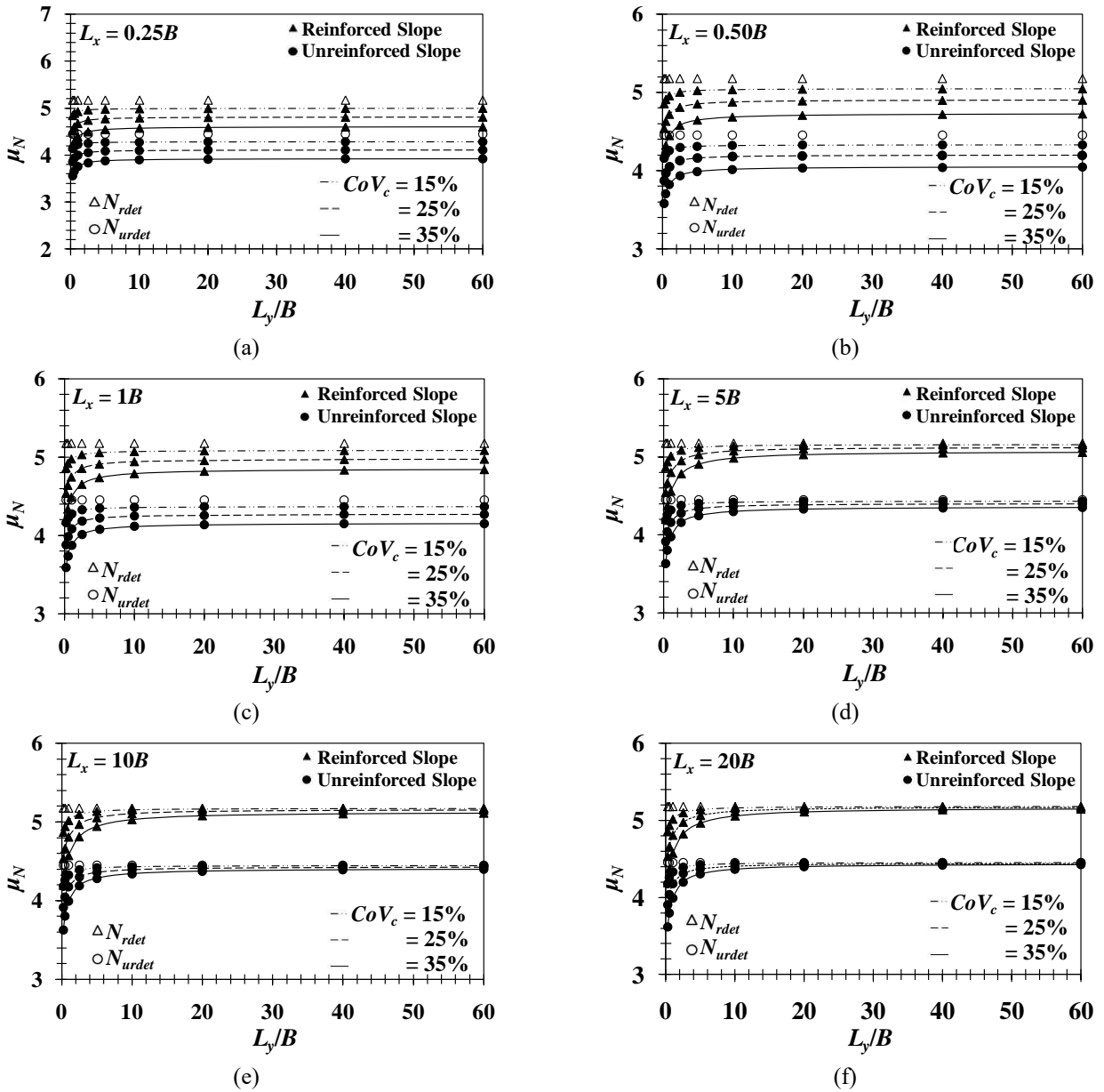


Fig. 6 Variation between  $\mu_N$ ,  $L_y/B$ , and  $CoV_c$  for unreinforced and reinforced slope of  $\beta = 30^\circ$  with  $L_x/B =$  (a) 0.25, (b) 0.50, (c) 1, (d) 5, (e) 10, (f) 20, (g) 40 and (h) 60

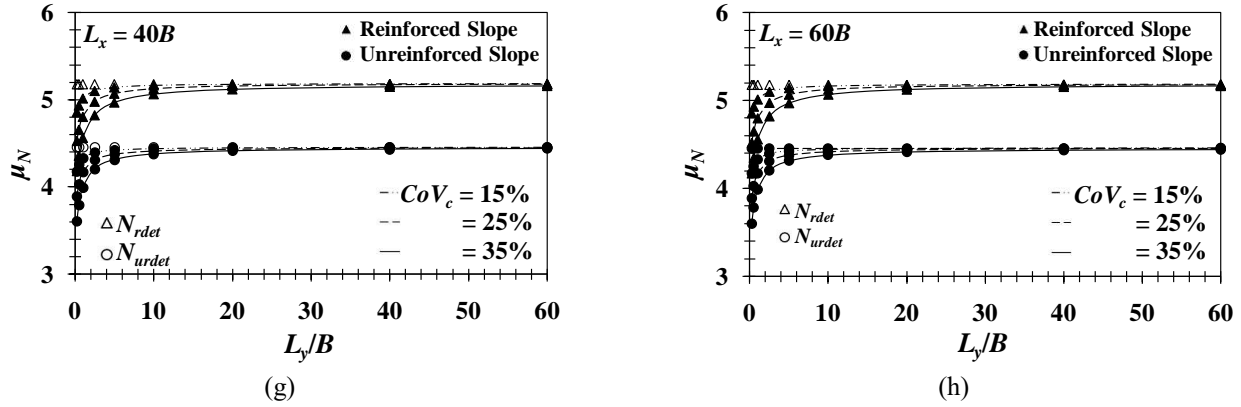


Fig. 6 Continued

combinations of  $CoV_c$ ,  $L_x$ , and  $L_y$ . When the values of  $L_x$  and  $L_y$  are small ( $L_x = 0.25B$  and  $L_y = 0.25B$ ), the spatial distribution plot in Fig. 3(a) shows variation of  $c$  is very much disperse in both the directions. With the increasing values of  $CoV_c$  (25% and 35%) and constant values of  $L_x = 0.25B$  and  $L_y = 0.25B$ , the range of variation of the spatial value of  $c$  increases. (Refer to Fig. 3b-c). On the other hand, Figs. 3(d-e) illustrate that with the increment in the  $L_y$  value but keeping  $CoV_c$  and  $L_x$  as constant, the spatial plot of  $c$  becomes more or less uniformly distributed only in the vertical direction rather than sparsely distributed in both the horizontal and vertical directions.

### 5.2 Deterministic analysis

The effectiveness of reinforcement in increasing the value of  $N$  ( $= Q_{ur}/cB$ ) for a strip footing under vertical load is indicated by Fig. 4(a). With the inclusion of a single layer of reinforcement, the magnitude of  $N$  increases. The maximum reinforcing efficiency ( $\eta_{max-det}$ ) is obtained after placing reinforcement at a critical depth ( $d_{cr}$ ). Beyond that depth, reinforcing efficacy reduces to unity. As an instance, the value of  $\eta_{max-det}$  is found to be 1.17 at a value of  $d_{cr}/B = 0.26$  for a slope with  $\beta = 20^\circ$ . When the reinforcement layer is laid at that critical depth, it distributes stresses into a wider and deeper area below the footing. If the depth of placement is more than the value of  $d_{cr}$ , stresses generated below the footing do not extend up to the depth of the reinforcement layer; it passes by touching the reinforcement layer. The effectiveness of the reinforcement increases slightly with the increase in the value of slope angle.

Fig. 4(b) shows that the inclusion of reinforcement layer is also found to be useful for footing under eccentric loading. If a single layer of reinforcement is placed at the critical depth, the magnitude of  $N$  increases with respect to the value of  $N$  for unreinforced slope. However, the magnitude of  $\eta_{det}$  reduces with the loading eccentricity for reinforced slope.

### 5.3 Probabilistic analysis

Figs. 5 and 6 show the variation between the mean values of  $N$  ( $\mu_N$ ) with  $CoV_c$  and  $L_y/B$  for both unreinforced and reinforced slopes with inclination of  $20^\circ$  and  $30^\circ$ . In

Figs. 5 and 6, design charts are presented for  $L_x$  values of  $0.25B$ ,  $0.50B$ ,  $1B$ ,  $5B$ ,  $10B$ ,  $20B$ ,  $40B$ , and  $60B$ . With the inclusion of a single layer of reinforcement in a slope, the magnitude of  $\mu_N$  increases. As shown in Fig. 5(a), the value of  $\mu_N$  increases from 3.98 to 4.58 after laying a single layer of reinforcement in a slope with  $\beta = 20^\circ$ ,  $CoV_c = 35\%$ ,  $L_x = 0.25B$ , and  $L_y = 1B$ . For both unreinforced and reinforced slopes, the magnitude of  $\mu_N$  reduces with the increasing randomness in the soil shear strength. Fig. 5 illustrates that the value of  $\mu_N$  reduces by a margin of 13.40% with the change in the magnitude of  $CoV_c$  from 15% to 35% for a reinforced slope with a combination of  $\beta = 20^\circ$ ,  $L_x = 0.25B$ , and  $L_y = 0.25B$ . For smaller correlation lengths, the value of  $\mu_N$  obtained from the probabilistic analysis of both unreinforced and reinforced slopes is always lower than the deterministic solution, which implies that the deterministic analysis always overestimates. However, with the increment in the correlation lengths, this difference reduces and at a higher correlation length the deterministic  $N$  values and probabilistic mean  $N$  ( $\mu_N$ ) values of both unreinforced and reinforced slopes become almost equal. Spatial plots in Fig. 3 for smaller values of  $L_x$  and  $L_y$  also indicate randomness in the value of  $c$ . On the other hand, spatial distribution plots in Fig. 3 for larger values of  $L_y$  indicate less randomness in the value of  $c$ , which is quite similar to the consideration of uniformly varied undrained shear strength in deterministic analysis. Therefore, the consideration of spatial variability in the determination of  $N$  for a strip footing placed on the edge of both unreinforced and reinforced slopes is essential. As an instance, for a reinforced slope with  $\beta = 30^\circ$ ,  $CoV_c = 35\%$ , and  $L_x = 0.25B$ , the value of  $\mu_N$  changes from 4.18 to 4.49 with the change in the value of  $L_y$  from  $0.25B$  to  $2.5B$  and then it reaches the  $N_{r-det}$  value of 4.57 when  $L_y$  becomes equal to  $10B$ . Similar to the deterministic analysis, value of  $\mu_N$  for both unreinforced and reinforced slope reduces with the increment in the value of slope inclination. By keeping the values of  $CoV_c = 25\%$ ,  $L_x = 1B$ , and  $L_y = 5B$  as constant, the magnitude of  $\mu_N$  is found to be reduced from 5.10 to 4.90 when the slope inclination of the reinforced slope increases from  $20^\circ$  to  $30^\circ$ .

Figs. 7(a)-7(d) illustrate the variation between the magnitude of the coefficient of variation of  $N$  ( $CoV_N$ ) with  $CoV_c$  and  $L_y/B$  for both unreinforced and reinforced slopes

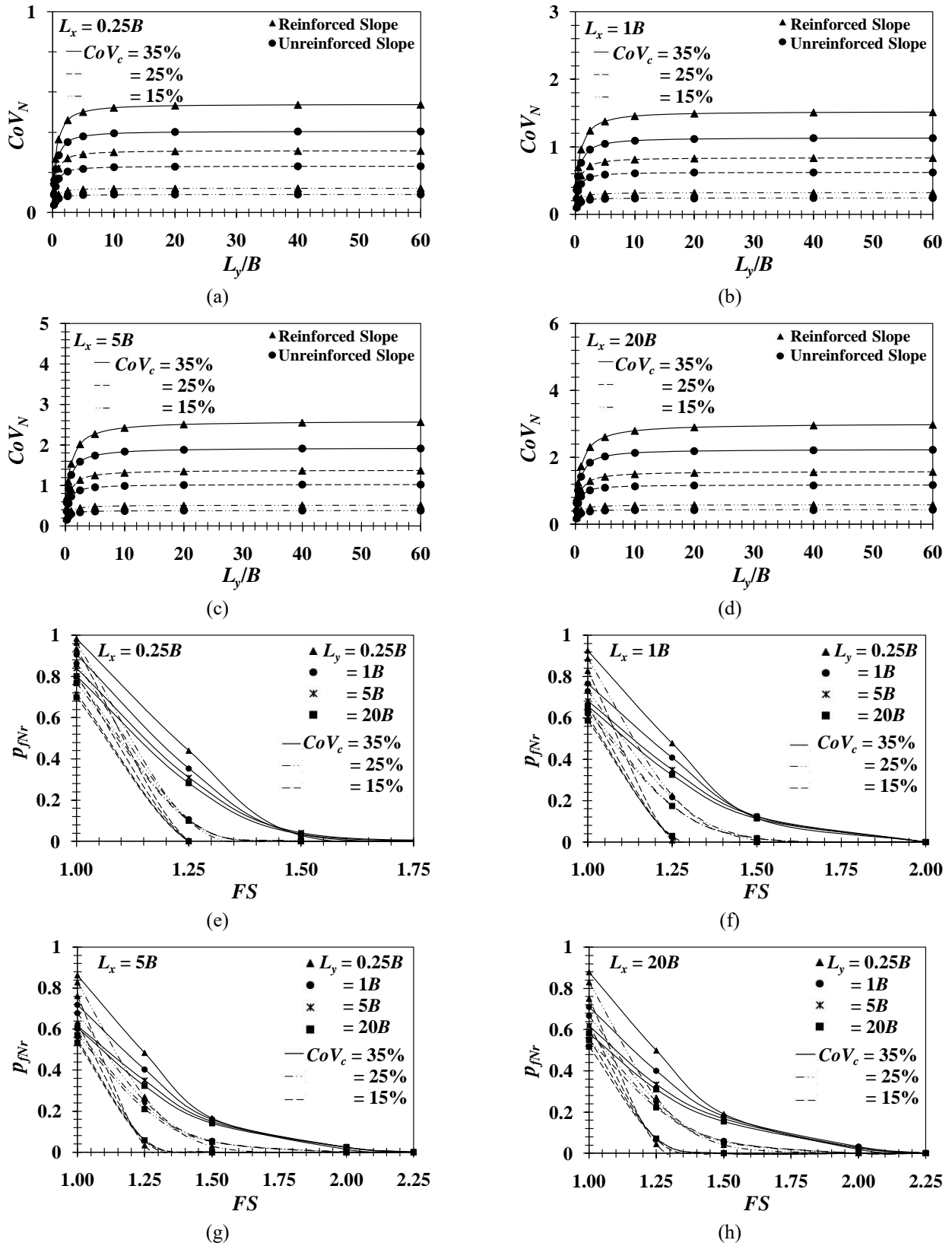


Fig. 7 Variation of  $CoV_N$ ,  $L_y/B$ , and  $CoV_c$  for unreinforced and reinforced slope of  $\beta = 20^\circ$  with  $L_x/B =$  (a) 0.25, (b) 1, (c) 5, (d) 20, variation of  $p_{fNr}$  with  $FS$ ,  $L_y$ , and  $CoV_c$  for reinforced slope of  $\beta = 20^\circ$  with  $L_x/B =$  (e) 0.25, (f) 1, (g) 5 and (h) 20

with  $\beta = 20^\circ$  and  $L_x/B = 0.25, 1, 5,$  and  $20$ . One can also obtain the same design charts for  $\beta = 30^\circ$  by the same methodology. The magnitude of  $CoV_N$  increases rapidly for

the smaller values of  $L_x$  and  $L_y$ , mostly within the range of  $1B$  to  $2.5B$  depending upon the value of  $CoV_c$ . After that range of  $L_x$  and  $L_y$ , the magnitude of  $CoV_N$  becomes almost

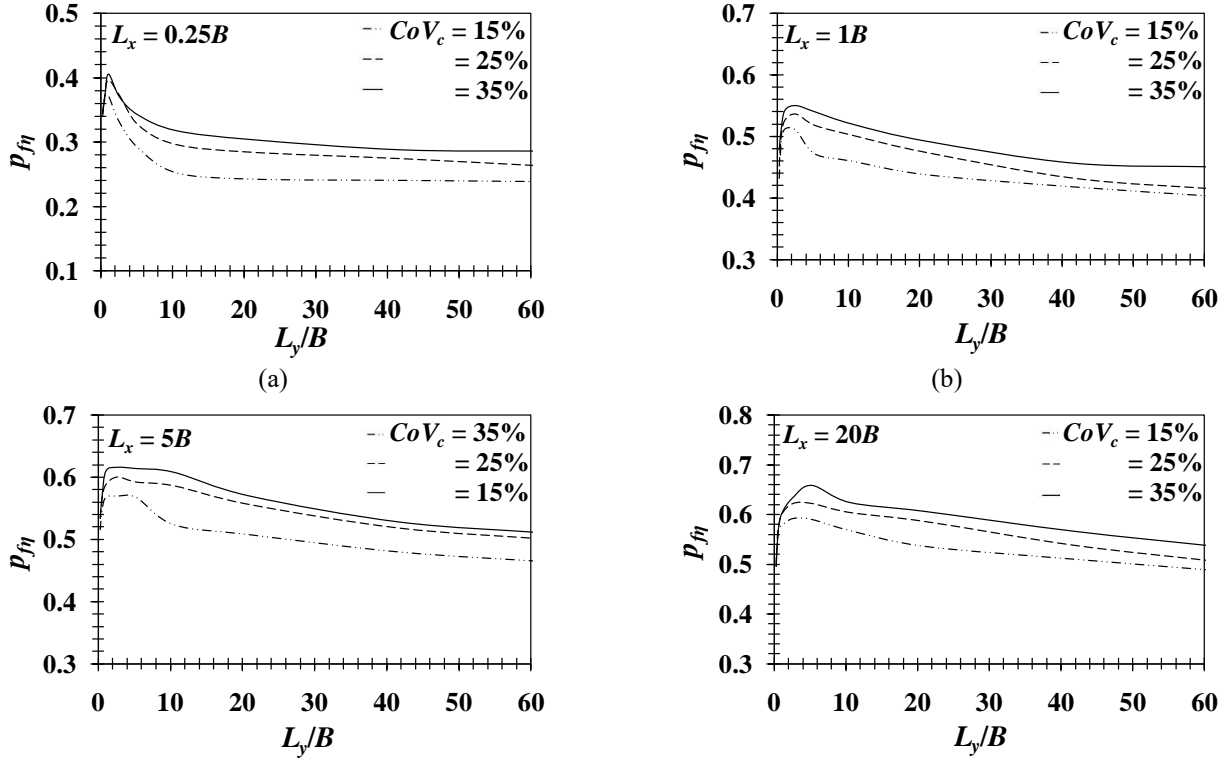


Fig. 8 Variation of  $p_{fh}$  with  $L_y/B$  and  $CoV_c$  for reinforced slope of  $\beta = 20^\circ$  with  $L_x/B =$  (a) 0.25, (b) 1, (c) 5 and (d) 20

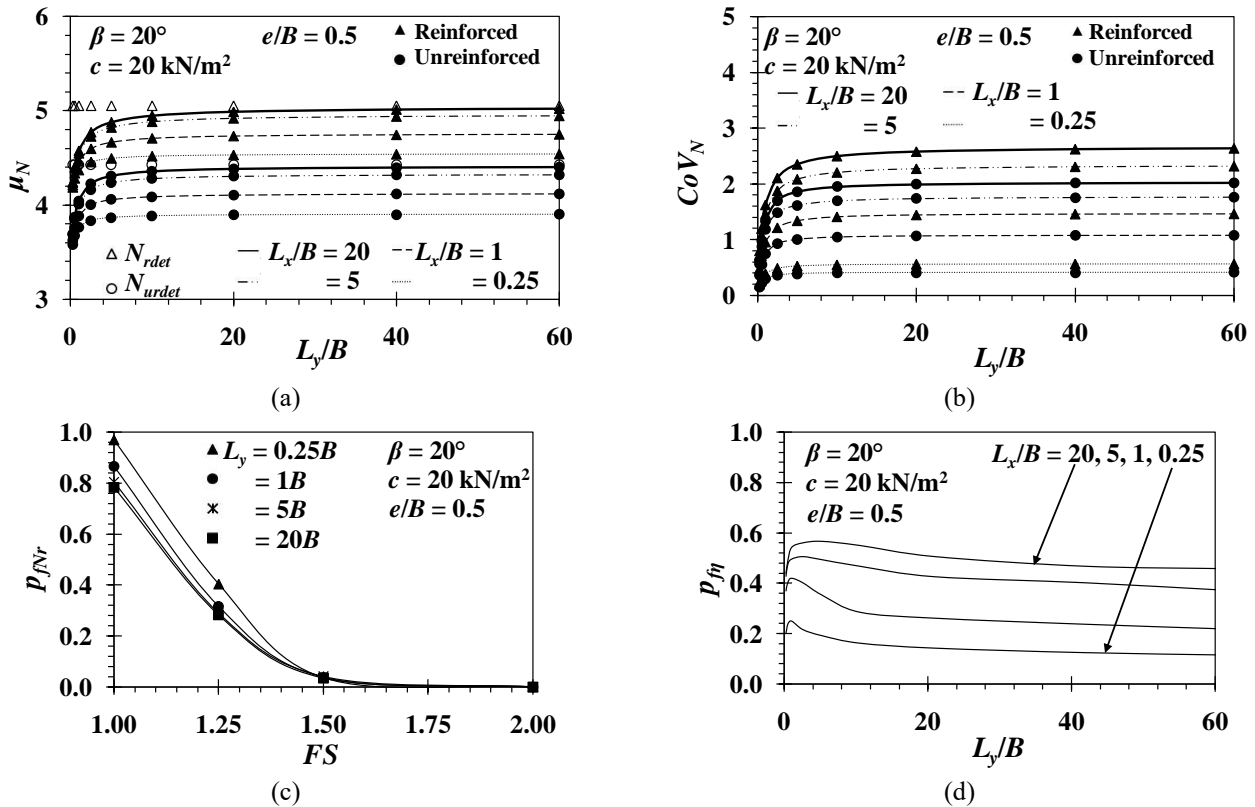


Fig. 9 (a) Variation of  $\mu_N$  with  $L_x/B$  and  $L_y/B$  for unreinforced and reinforced slope of  $\beta = 20^\circ$ ,  $e/B = 0.5$ , and  $CoV_c = 35\%$ , (b) variation of  $CoV_N$  with  $L_x/B$  and  $L_y/B$  for unreinforced and reinforced slope of  $\beta = 20^\circ$ ,  $e/B = 0.5$ , and  $CoV_c = 35\%$ , (c) variation of  $p_{fNr}$  with  $FS$ ,  $L_x/B$  and  $L_y/B$  for reinforced slope of  $\beta = 20^\circ$ ,  $e/B = 0.5$ , and  $CoV_c = 35\%$  and (d) variation of  $p_{fh}$  with  $L_x/B$  and  $L_y/B$  for reinforced slope of  $\beta = 20^\circ$ ,  $e/B = 0.5$ , and  $CoV_c = 35\%$

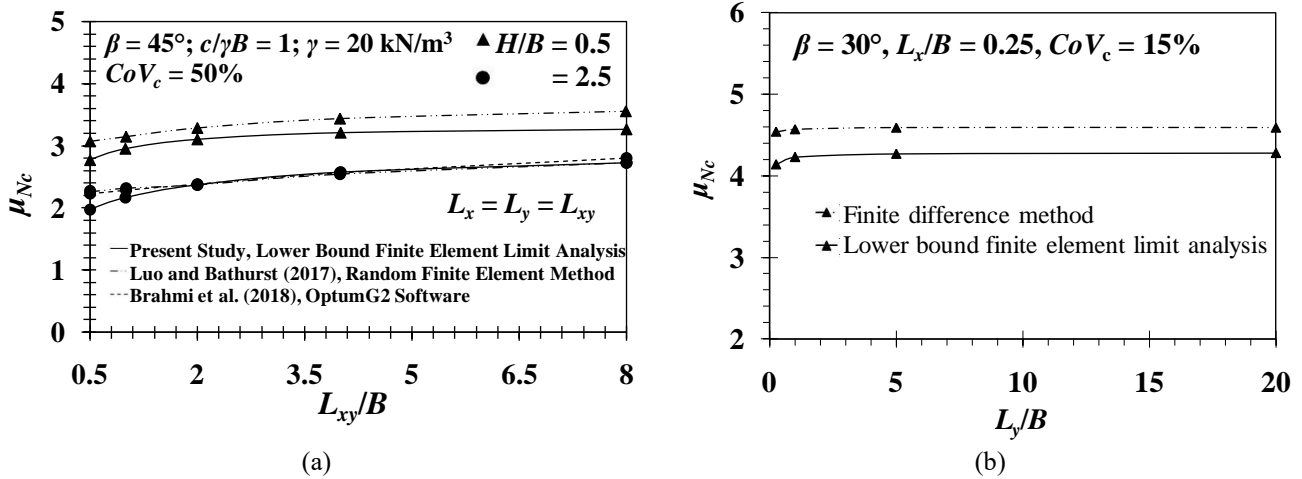


Fig. 10 (a) Comparison between the obtained values of  $\mu_{Nc}$  and  $L_{xy}/B$  from the present study and other research studies and (b) comparison between the obtained values of  $\mu_{Nc}$  from finite difference method and lower bound finite element limit analysis

constant with the increasing value of  $L_x$  and  $L_y$ . As an example for a reinforced slope having a combination of  $\beta = 20^\circ$ ,  $CoV_c = 15\%$ , and  $L_x = 0.25B$ , the magnitude of  $CoV_N$  leaps from a value of 0.04 to 0.08 with the change in  $L_y$  value from  $0.25B$  to  $2.5B$ . After that, the magnitude of  $CoV_N$  reaches a constant value of 0.09. The magnitude of  $CoV_N$  for both unreinforced and reinforced slope enhances with the increment in the magnitude of  $CoV_c$ . However, for all the combinations of  $CoV_c$ ,  $L_x$ , and  $L_y$ , the value of  $CoV_N$  obtained for reinforced slope is always higher than the value of  $CoV_N$  obtained for unreinforced slope.

The variation between the failure probability ( $p_{fNr}$ ) of  $N$  obtained for reinforced slope and its factor of safety ( $FS$ ) for  $\beta = 20^\circ$  and various combinations of  $CoV_c$ ,  $L_x$ , and  $L_y$  is illustrated in Figs. 7(e) and 7(h). Four values of  $L_x/B = 0.25$ , 1, 5, and 20 are considered. With an increment in  $FS$  value, the magnitude of  $p_{fNr}$  reduces. As an instance, for a slope with  $\beta = 20^\circ$ ,  $CoV_c = 35\%$ ,  $L_x = 0.25B$  and  $L_y = 0.25B$ , the magnitude of  $p_{fNr}$  reduces from 0.98 to 0.03 with the increment in  $FS$  value from 1.00 to 1.50. It is to be noted that the magnitude of  $p_{fNr}$  reduces with the increase in the value of  $L_x$  and  $L_y$  for a particular value of  $\beta$ ,  $CoV_c$ , and  $FS$ . The magnitude of  $p_{fNr}$  for a slope of  $\beta = 20^\circ$ ,  $L_x = 0.25B$ ,  $CoV_c = 35\%$ , and  $FS = 1$ , decreases from 0.98 to 0.80 as  $L_y$  value varies between  $0.25B$  and  $20B$ .

The variation of the failure probability ( $p_{f\eta}$ ) of the efficiency factor  $\eta$  of a reinforced slope with different values of  $CoV_c$ , and  $L_y$  is presented in Figs. 8(a-d). Design charts are provided for  $\beta = 20^\circ$  with  $L_x/B = 0.25$ , 1, 5, and 20. For a particular magnitude of  $CoV_c$ , the magnitude of  $p_{f\eta}$  increases up to a particular value of  $L_x$  and  $L_y$  and after attaining maximum value it reduces and then remains constant with the increasing value of  $L_x$  and  $L_y$ . The range of  $L_x$  and  $L_y$  at which  $p_{f\eta}$  attains the peak value varies between  $1B$  to  $2.5B$  for all the analyses depending upon the values of  $\beta$  and  $CoV_c$ . The magnitude of  $p_{f\eta}$  enhances with the increasing value of soil randomness characteristics such as  $CoV_c$ ,  $L_x$  and  $L_y$ . For a slope inclination of  $20^\circ$ ,  $L_x = 1B$ , and  $L_y = 0.25B$ , the failure probability of the efficiency factor increases from 0.43 to 0.48 with the increment in the

magnitude of  $CoV_c$  from 15% to 35%.

Results associated with the strip footing under eccentric load are shown in Fig. 9. The  $L_x/B$  values are chosen as 0.25, 1, 5, and 20. The change in the value of  $\mu_N$  with  $L_y/B$  for both unreinforced and reinforced slopes with  $\beta = 20^\circ$  and  $CoV_c = 35\%$  are illustrated in Fig. 9(a). For all the combinations of  $\beta$ ,  $L_x$ ,  $L_y$ , and  $CoV_c$ , the probabilistic bearing capacity of a strip footing under eccentric load is always lesser in comparison to a strip footing subjected to vertical load. As an instance, for a reinforced slope with  $\beta = 20^\circ$ ,  $L_x/B = 0.25$ ,  $L_y/B = 1.0$ , and  $CoV_c = 35\%$ , the magnitude of  $\mu_N$  of the strip footing under eccentric and vertical loading is 4.37 and 4.58, respectively. Probabilistic bearing capacity also increases with a inclusion of a single layer of reinforcement. The magnitude of  $\mu_N$  of a slope with  $\beta = 20^\circ$ ,  $L_x/B = 0.25$ ,  $L_y/B = 1.0$ , and  $CoV_c = 35\%$  increases from 3.76 to 4.37 with the inclusion of a single layer of reinforcement. Fig. 9(b) shows that the magnitude of  $CoV_N$  increases rapidly for the smaller values of  $L_x$  and  $L_y$ . After that, the magnitude of  $CoV_N$  becomes almost constant with the increasing value of  $L_x$  and  $L_y$ . Fig. 9(c) shows that the magnitude of  $p_{fNr}$  associated with a reinforced slope of  $\beta = 20^\circ$ ,  $L_x/B = 0.25$ ,  $L_y/B = 1.0$ , and  $CoV_c = 35\%$  reduces from 0.87 to 0.04 with the increment in the value of  $FS$  from 1.0 to 1.5. Beyond a particular  $L_y/B$  value, the increment in the failure probability ( $p_{f\eta}$ ) of the efficiency factor  $\eta$  of a reinforced slope under eccentric loading becomes insignificant. Fig. 9(d) shows that the coefficient of variation of the bearing capacity factor  $N$  ( $CoV_N$ ) increases rapidly for the smaller values of  $L_y$ , after that it becomes almost constant. The value of  $CoV_N$  associated with reinforced slope is always higher for any combinations of  $\beta$ ,  $L_x$ ,  $L_y$ , and  $CoV_c$ . Similar to footing under vertical load, the failure probability of the bearing capacity factor reduces as the factor of safety increases.

#### 5.4 Comparison

Until now, no studies estimated the probabilistic bearing capacity of a strip foundation resting on top of a purely

cohesive reinforced soil slope. Hence, the probabilistic results obtained from the present study are compared with the available probabilistic results of (i) Luo and Bathurst (2017) and (ii) Brahmi *et al.* (2018) obtained for the strip footing placed on the unreinforced soil slope of  $\beta = 45^\circ$ . Luo and Bathurst (2017) used Random Finite Element Method to calculate the probabilistic bearing capacity factor related to soil cohesion ( $N_c$ ) of the strip footing. Whereas, Brahmi *et al.* (2018) used commercially available software OptumG2 to obtain the lower bound value of the  $N_c$  for the strip footing. It is to be mentioned that both Luo and Bathurst (2017) and Brahmi *et al.* (2018) modelled soil shear strength as an isotropic random field ( $L_x = L_y = L_{xy}$ ). Fig. 10(a) shows comparison between present lower bound values of  $N_c$  ( $\mu_{N_c}$ ) with (i) Luo and Bathurst (2017) for the slope height ( $H$ ) of  $0.5B$  and  $2.5B$  and (ii) Brahmi *et al.* (2018) for the slope height ( $H$ ) of  $2.5B$ . Correlation length ( $L_{xy}$ ) is varied from  $0.50B$  to  $8B$ . Following Luo and Bathurst (2017) and Brahmi *et al.* (2018), magnitudes of various parameters are considered as  $c/\gamma B = 1$ ;  $\gamma = 20$  kN/m<sup>3</sup>; and  $CoV_c = 50\%$ . It is found out that for the slope height of  $2.5B$ , the magnitude of  $\mu_{N_c}$  obtained from the present study is slightly lower than that presented by Luo and Bathurst (2017) and Brahmi *et al.* (2018) for smaller values of correlation length. However, the present solution matches very well with the solutions of Luo and Bathurst (2017) and Brahmi *et al.* (2018) for higher values of correlation length. The present lower bound solution of  $\mu_{N_c}$  for slope height ( $H/B$ ) of  $0.5$  is always on the lower side of the solution provided by Luo and Bathurst (2017).

Present methodology is further validated by comparing the values of probabilistic bearing capacity factor obtained from the lower bound limit analysis technique and finite difference method by using Fast Lagrangian Analysis of Continua (FLAC) software. Fig. 10(b) shows the variation in the values of  $\mu_{N_c}$  for a strip footing placed on an unreinforced soil slope of  $\beta = 30^\circ$ . Probabilistic parameters are considered as:  $L_x/B = 0.25$ ,  $L_y/B = 0.25, 1, 5$ , and  $20$ , and  $CoV_c = 15\%$ . It is found that the values of  $\mu_{N_c}$  obtained from lower bound limit analysis technique is always lower than that obtained from the finite difference method. However, the trend of variation is similar in both of these methods.

On the other hand, the validation of the reinforcement modelling is carried out by comparing the deterministic results obtained for the (i) reinforced horizontal clayey ground and (ii) reinforced soil slope. For the comparison with results of reinforced horizontal clayey ground, experimental results of (i) Shin *et al.* (1993) and (ii) Das *et al.* (1994) and numerical result of Chakraborty and Kumar (2014) are considered. Present results are compared for both single and double reinforced horizontal ground and detailed in Table 1. It is to be noted that Chakraborty and Kumar (2014) used lower bound limit analysis with linear optimization. Efficacy of reinforcement layer is presented by a dimensionless factor ( $\eta_{cdet} = N_{cr}/N_{cur}$ ), where  $N_{cr}$  and  $N_{cur}$  are bearing capacity factor for unreinforced and reinforced ground. The magnitude of  $\eta_{cdet}$  obtained from the present study for both single and double reinforced horizontal ground matches well with the solution of

Table 1 Comparison between results obtained from present study and available literature for clay ( $\phi = 0^\circ$ )

Reference	Layers of Reinforcement				
	Single		Two		
	$d_1/B$	$\eta_{cdet}$	$d_1/B$	$d_2/B$	$\eta_{cdet}$
Present Study (Lower bound limit analysis with conic optimization)	0.34	1.10	0.30	0.36	1.16
Chakraborty and Kumar (2014) (Lower bound limit analysis with linear optimization)	0.36	1.09	0.36	0.36	1.15
Shin <i>et al.</i> (1993) (Experimental analysis)	0.4	1.11	0.4	0.33	1.23
Das <i>et al.</i> (1994) (Experimental analysis)	0.4	1.09	0.4	0.33	1.21

Table 2 Comparison between present result and available result from Lee and Manjunath (2000)

Slope configuration	Reference	Maximum reinforcing efficiency	
		Experimental	Numerical
$\beta = 26.56^\circ$ , $\phi = 38^\circ$ , $b/B = 1$ , $d_{1cr}/B = 0.50$ , $N_r = 1$ (single reinforcement)	Present Study (Lower bound limit analysis with conic optimization)	-	1.81
	Lee and Manjunath (2000)	1.76	1.80 (PLAXIS)

Chakraborty and Kumar (2014). On the other hand, the present value of  $\eta_{cdet}$  is always on the lower side with respect to the experimental values of (i) Shin *et al.* (1993) and (ii) Das *et al.* (1994).

Present result is also compared with the experimental and numerical results of Lee and Manjunath (2000) obtained for a strip footing placed at a edge distance of  $B$  ( $b/B = 1$ ) on the reinforced soil slope. The comparison is detailed in Table 2. Lee and Manjunath (2000) used finite element software PLAXIS for carrying out numerical analysis. It is found that value of maximum efficiency factor obtained from the present study is slightly higher than the experimental result of Lee and Manjunath (2000). On the other hand, maximum reinforcing efficiency obtained from the present study is almost equal to the reported numerical value of maximum reinforcing efficiency factor in Lee and Manjunath (2000).

## 6. Failure patterns

Failure mechanisms of both unreinforced and reinforced slopes are obtained from both deterministic and probabilistic analyses. Failure state of stress of any point is plotted with respect to the two-dimensional problem domain. The state of stress of any point at the time of collapse is expressed by a dimensionless term,  $a/f$ ; where  $a = (\sigma_x - \sigma_y)^2 + (\tau_{xy})^2$  and  $f = 4c^2$ . Unity value of  $a/f$  at any point denotes yielding of that point. Non-yielding is denoted by the value of  $a/f < 1$ . Figs. 11(a) and 11(b) show the failure patterns of unreinforced and reinforced slopes

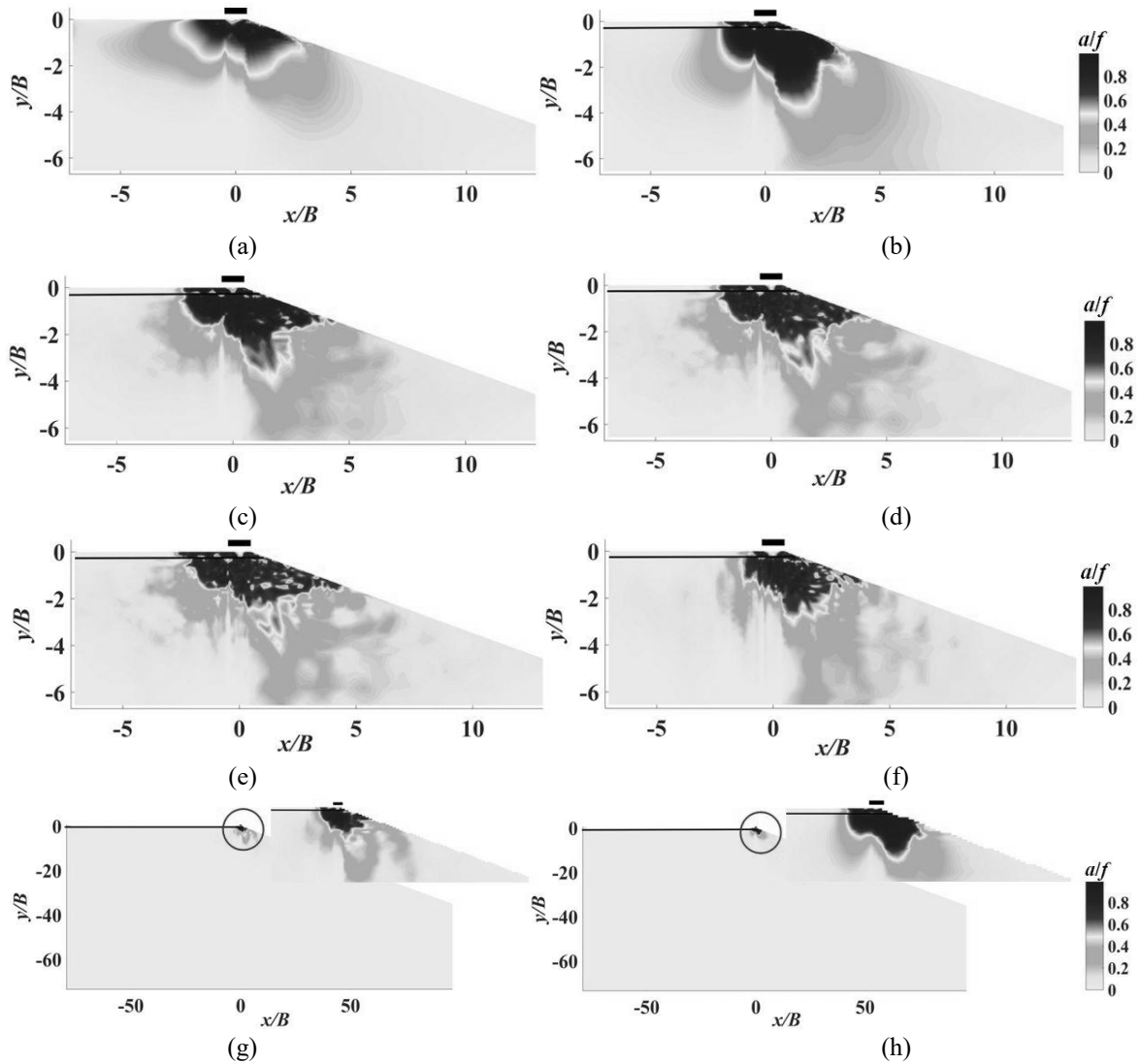


Fig. 11 Failure patterns obtained for (a) unreinforced slope with  $\beta = 20^\circ$ , (b) reinforced slope with  $\beta = 20^\circ$ ,  $d_{cr}/B = 0.26$ ;  $\eta_{c-det} = 1.15$ , (c) reinforced slope with  $\beta = 20^\circ$ ,  $CoV_c = 15\%$ ,  $L_x/B = 0.25$ ;  $L_y/B = 0.25$ , (d) reinforced slope with  $\beta = 20^\circ$ ,  $CoV_c = 25\%$ ,  $L_x/B = 0.25$ ;  $L_y/B = 0.25$ , (e) reinforced slope with  $\beta = 20^\circ$ ,  $CoV_c = 35\%$ ,  $L_x/B = 0.25$ ;  $L_y/B = 0.25$ , (f) reinforced slope with  $\beta = 20^\circ$ ,  $CoV_c = 35\%$ ,  $L_x/B = 0.25$ ;  $L_y/B = 5$ , (g) reinforced slope with  $\beta = 20^\circ$ ,  $CoV_c = 35\%$ ,  $L_x/B = 0.25$ ;  $L_y/B = 40$  and (h) reinforced slope with  $\beta = 20^\circ$ ,  $CoV_c = 35\%$ ,  $L_x/B = 40$ ,  $L_y/B = 40$

obtained from the deterministic study. It is clearly visible that for both the unreinforced and reinforced slopes, the failure surface propagates easily towards the slope face side. However, with the inclusion of reinforcement layer stresses propagate more in the downward direction in comparison to the unreinforced slope, then it reaches to the slope face. Failure patterns are also plotted for slope having different combinations of spatially variable soil shear strength as depicted in Figs. 3(a)-3(e). When the correlation lengths in  $x$  and  $y$  directions are very less ( $L_x = L_y = 0.25B$ ), failure patterns of the reinforced slope become very disperse (refer: Fig. 11(c)) with respect to the deterministic case (refer: Fig. 11(b)) and with the higher value of  $CoV_c$ , dispersion in the failure pattern increases (refer: Figs. 11(d) and 11(e)). The dispersion in the failure patterns are obvious as lower values of correlation length indicate more randomness and with the increment in the magnitude of  $CoV_c$ , randomness increases. However, with the increment

in the magnitude of correlation length, failure pattern tends to be smooth (refer: Figs. 11(f) and 11(g)). As the magnitude of  $L_x$  and  $L_y$  becomes very high ( $L_x = L_y = 40B$ ) which is similar to the case of the slope where soil shear strength value is constant, failure pattern becomes almost smooth rather than being dispersed (refer: Fig. 11(h)).

## 7. Remarks

(i) The mean value of the undrained shear strength of soil is considered as  $20 \text{ kN/m}^2$ . Expression for dimensionless bearing capacity factor  $N (= Q_u/cB)$  indicates that the ultimate collapse load changes with the change in the magnitude of  $c$  which in turn makes the non-dimensional factor  $N$  independent on the value of  $c$ . Thus, design engineers can use the present design charts for any other values of  $c$ .

(ii) Present study only predicts the lower bound bearing capacity of strip footing placed on a purely cohesive soil slope. However, a true solution always lies in between upper and lower bound values.

## 8. Conclusions

Outcomes of the present study will contribute to practical methodologies and guidelines to account the spatial variability and randomness in undrained soil shear strength in the investigation of behaviour of strip footing placed on a reinforced cohesive soil slope. Utilizing the design charts presented in this study, practicing engineers can predict the bearing capacity of strip footing for different combinations of slope angle, loading conditions and material heterogeneity. Salient features of the present study are detailed below.

- For the smaller correlation lengths, the mean of the probabilistic bearing capacity factor is noted to be much smaller in comparison to the deterministic bearing capacity factor of the strip footing placed on both unreinforced and reinforced soil slope. With the increment in the value of  $CoV_c$ , difference in the magnitude of probabilistic and deterministic bearing capacity further increases. However, with the increment in the value of  $L_x$ , and  $L_y$ , the magnitude of the mean value of dimensionless probabilistic bearing capacity factor approaches to the deterministic  $N$  value.

- Failure probability of the  $N$  associated with the strip footing placed on the reinforced slope ( $p_{Nr}$ ) is found to be reducing constantly with the increase in the value of factor of safety. Failure of the efficiency factor ( $p_{\eta}$ ) is also obtained and found that the magnitude of  $p_{\eta}$  increases up to a certain value of  $L_x$  and  $L_y$  and after attaining maximum value it becomes almost constant with the increasing value of  $L_x$  and  $L_y$ .

- The probabilistic bearing capacity factor obtained for the unreinforced and reinforced slopes under eccentric loading is always lesser than that obtained for unreinforced and reinforced slopes under vertical loading.

## Acknowledgments

The authors gratefully acknowledge the Department of Science and Technology, Government of India for their financial support vide Science and Engineering Research Board (SERB) research project grant number DST No: SB/FTP/ETA-0061/2014 dated 17/07/2014.

## References

- Abd, A.H. and Utili, S. (2017), "Design of geosynthetic-reinforced slopes in cohesive backfills", *Geotext. Geomembr.*, **45**(6), 627-641. <https://doi.org/10.1016/j.geotextmem.2017.08.004>.
- Brahmi, N., Ouahab, M.Y., Mabrouki, A., Benmeddour, D. and Mellas, M. (2018), "Probabilistic analysis of the bearing capacity of inclined loaded strip footings near cohesive slopes", *Int. J. Geotech. Eng.*, 1-8. <https://doi.org/10.1080/19386362.2018.1496005>.
- Chakraborty, D. and Kumar, J. (2014), "Bearing capacity of strip foundations in reinforced soils", *Int. J. Geomech.*, **14**(1), 45-58. [https://doi.org/10.1061/\(ASCE\)GM.1943-5622.0000275](https://doi.org/10.1061/(ASCE)GM.1943-5622.0000275).
- Chen, Y., Gao, Y., Yang, S. and Zhang, F. (2018), "Required unfactored geosynthetic strength of three-dimensional reinforced soil structures comprised of cohesive backfills", *Geotext. Geomembr.*, **46**(6), 860-868. <https://doi.org/10.1016/j.geotextmem.2018.08.004>.
- Das, B.M., Shin, E.C. and Omar, M.T. (1994), "The bearing capacity of surface strip foundations on geogrid-reinforced sand and clay—a comparative study", *Geotech. Geol. Eng.*, **12**(1), 1-14. <https://doi.org/10.1007/BF00425933>.
- Ghanbari, A., Khalilpasha, A., Sabermahani, M. and Heydari, B. (2013), "An analytical technique for estimation of seismic displacements in reinforced slopes based on horizontal slices method (HSM)", *Geomech. Eng.*, **5**(2), 143-164. <http://doi.org/10.12989/gae.2013.5.2.143>.
- Griffiths, D.V., Fenton, G.A. and Manoharan, N. (2002), "Bearing capacity of rough rigid strip footing on cohesive soil: Probabilistic study", *J. Geotech. Geoenviron. Eng.*, **128**(9), 743-755. [https://doi.org/10.1061/\(ASCE\)1090-0241\(2002\)128:9\(743\)](https://doi.org/10.1061/(ASCE)1090-0241(2002)128:9(743)).
- Haldar, A. and Mahadevan, S. (2000), *Probability, Reliability, and Statistical Methods in Engineering Design*, Wiley, New York, U.S.A.
- Halder, K. and Chakraborty, D. (2018), "Bearing capacity of strip footing placed on the reinforced soil slope", *Int. J. Geomech.*, **18**(11), 06018025. [https://doi.org/10.1061/\(ASCE\)GM.1943-5622.0001278](https://doi.org/10.1061/(ASCE)GM.1943-5622.0001278).
- Halder, K. and Chakraborty, D. (2019a), "Effect of interface friction angle between soil and reinforcement on bearing capacity of strip footing placed on reinforced slope", *Int. J. Geomech.*, **19**(5), 06019008. [https://doi.org/10.1061/\(ASCE\)GM.1943-5622.0001394](https://doi.org/10.1061/(ASCE)GM.1943-5622.0001394).
- Halder, K. and Chakraborty, D. (2019b), "Seismic bearing capacity of strip footing placed on the reinforced slope", *Geosynth. Int.*, **26**(5), 474-484. <https://doi.org/10.1680/jgein.19.00032>.
- Halder, K. and Chakraborty, D. (2019c), "Probabilistic bearing capacity of strip footing on reinforced soil slope", *Comput. Geotech.*, **116**, 1-11. <https://doi.org/10.1016/j.compgeo.2019.103213>.
- Halder, K. and Chakraborty, D. (2020), "Influence of soil spatial variability on the response of strip footing on geocell reinforced slope", *Comput. Geotech.*, **122**, 1-13. <https://doi.org/10.1016/j.compgeo.2020.103533>.
- Halder, K., Chakraborty, D. and Dash, S.K. (2019), "Bearing capacity of a strip footing situated on soil slope using a non-associated flow rule in lower bound limit analysis", *Int. J. Geotech. Eng.*, **13**(2), 103-111. <https://doi.org/10.1080/19386362.2017.1325119>.
- Huang, C. and Tatsuoka, F. (1994), "Stability analysis for footings on reinforced sand slopes", *Soils Found.*, **34**(3), 21-37. [https://doi.org/10.3208/sandf1972.34.3\\_21](https://doi.org/10.3208/sandf1972.34.3_21).
- ITASCA, FLAC 2D Version 7.0.411 (2011), *Fast Lagrangian Analysis of Continua in 2 Dimensions*, ITASCA Consulting Group Inc.
- Keskin, M.S. and Laman, M. (2014), "Experimental study of bearing capacity of strip footing on sand slope reinforced with tire chips", *Geomech. Eng.*, **6**(3), 249-262. <http://doi.org/10.12989/gae.2014.6.3.249>.
- Lee, K.M. and Manjunath, V.R. (2000), "Experimental and numerical studies of geosynthetic-reinforced sand slopes loaded with a footing", *Can. Geotech. J.*, **37**(4), 828-842. <https://doi.org/10.1139/t00-016>.
- Lombardi, M., Cardarilli, M. and Raspa, G. (2017), "Spatial variability analysis of soil strength to slope stability assessment", *Geomech. Eng.*, **12**(3), 483-503.

- <https://doi.org/10.12989/gae.2017.12.3.483>.
- Luo, N. and Bathurst, R.J. (2017), "Reliability bearing capacity analysis of footings on cohesive soil slopes using RFEM", *Comput. Geotech.*, **89**, 203-212.  
<https://doi.org/10.1016/j.compgeo.2017.04.013>.
- Luo, N. and Bathurst, R.J. (2018), "Deterministic and random FEM analysis of full-scale unreinforced and reinforced embankments", *Geosynth. Int.*, **25**(2), 164-179.  
<https://doi.org/10.1680/jgein.17.00040>.
- Makrodimopoulos, A. and Martin, C.M. (2006), "Lower bound limit analysis of cohesive-frictional materials using second-order cone programming", *Int. J. Numer. Meth. Eng.*, **66**(4), 604-634. <https://doi.org/10.1002/nme.1567>.
- MATLAB R2015a (2015), [Computer software]. Natick, MA, MathWorks.
- MOSEK ApS version 9.0 (n.d.) [Computer software]. MOSEK, Copenhagen, Denmark.
- Noorzad, R. and Mirmoradi, S.H. (2010), "Laboratory evaluation of the behavior of a geotextile reinforced clay", *Geotext. Geomembr.*, **28**(4), 386-392.  
<https://doi.org/10.1016/j.geotexmem.2009.12.002>.
- Phoon, K.K. and Kulhawy, F.H. (1999a), "Characterization of Geotechnical Variability", *Can. Geotech. J.*, **36**(4), 612-624.  
<https://doi.org/10.1139/t99-038>.
- Phoon, K.K. and Kulhawy, F.H. (1999b), "Evaluation of geotechnical property variability", *Can. Geotech. J.*, **36**(4), 625-639. <https://doi.org/10.1139/t99-039>.
- Pramanik, R., Baidya, D.K. and Dhang, N. (2019), "Implementation of fuzzy reliability analysis for elastic settlement of strip footing on sand considering spatial variability", *Int. J. Geomech.*, **19**(12), 04019126.  
[https://doi.org/10.1061/\(ASCE\)GM.1943-5622.0001514](https://doi.org/10.1061/(ASCE)GM.1943-5622.0001514).
- Selvadurai, A.P.S. and Gnanendran, C.T. (1989), "An experimental study of a footing located on a sloped fill: Influence of a soil reinforcement layer", *Can. Geotech. J.*, **26**(3), 467-473.  
<https://doi.org/10.1139/t89-059>.
- Shin, E.C., Das, B.M., Puri, V.K., Yen, S.C. and Cook, E.E. (1993), "Bearing capacity of strip foundation on geogrid-reinforced clay", *Geotech. Test. J.*, **16**(4), 534-541.  
[https://doi.org/10.1016/0266-1144\(94\)90066-3](https://doi.org/10.1016/0266-1144(94)90066-3).
- Sloan, S.W. (1988), "Lower bound limit analysis using finite elements and linear programming", *Int. J. Numer. Anal. Meth. Geomech.*, **12**(1), 61-77.  
<https://doi.org/10.1002/nag.1610120105>.
- Srivastava, A. and Sivakumar Babu, G.S. (2011), "Deflection and buckling of buried flexible pipe-soil system in a spatially variable soil profile", *Geomech. Eng.*, **3**(3), 169-188.  
<https://doi.org/10.12989/gae.2011.3.3.169>.
- Tang, C., Phoon, K.K. and Toh, K.C. (2014), "Lower-bound limit analysis of seismic passive earth pressure on rigid walls", *Int. J. Geomech.*, **14**(5), 04014022.  
[https://doi.org/10.1061/\(ASCE\)GM.1943-5622.0000385](https://doi.org/10.1061/(ASCE)GM.1943-5622.0000385).
- Turker, E., Sadoglu, E., Cure, E. and Uzuner, B.A. (2014), "Bearing capacity of eccentrically loaded strip footings close to geotextile-reinforced sand slope", *Can. Geotech. J.*, **51**(8), 884-895. <https://doi.org/10.1139/cgj-2014-0055>.
- Vahedifard, F., Leshchinsky, B.A., Sehat, S. and Leshchinsky, D. (2014), "Impact of cohesion on seismic design of geosynthetic-reinforced earth structure", *J. Geotech. Geoenviron. Eng.*, **140**(6), 04014016.  
[https://doi.org/10.1061/\(ASCE\)GT.1943-5606.0001099](https://doi.org/10.1061/(ASCE)GT.1943-5606.0001099).
- Wang, L., Zhang, G. and Zhang, J.M. (2011), "Centrifuge model tests of geotextile-reinforced soil embankments during an earthquake", *Geotext. Geomembr.*, **29**(3), 222-232.  
<https://doi.org/10.1016/j.geotexmem.2010.11.002>.
- Yang, S., Leshchinsky, B., Cui, K., Zhang, F. and Gao, Y. (2019), "Unified approach toward evaluating bearing capacity of shallow foundations near slope", *J. Geotech. Geoenviron. Eng.*, **145**(12), 04019110.  
[https://doi.org/10.1061/\(ASCE\)GT.1943-5606.0002178](https://doi.org/10.1061/(ASCE)GT.1943-5606.0002178).
- Yang, S., Leshchinsky, B., Cui, K., Zhang, F. and Gao, Y. (2020), "Influence of failure mechanism on seismic bearing capacity factors for shallow foundations near slopes", *Geotechnique*, 1-46. <http://doi.org/10.1680/jgeot.19.P.329>.
- Yoo, C. (2001), "Laboratory investigation of bearing capacity behaviour of strip footing on geogrid-reinforced sand slope", *Geotext. Geomembr.*, **19**(5), 279-298.  
[https://doi.org/10.1016/S0266-1144\(01\)00009-7](https://doi.org/10.1016/S0266-1144(01)00009-7).
- Yoo, C. (2016), "Effect of spatial characteristics of a weak zone on tunnel deformation behavior", *Geomech. Eng.*, **11**(1), 41-58.  
<http://dx.doi.org/10.12989/gae.2016.11.1.041>.
- Zheng, Y. and Fox, P.J. (2017), "Numerical investigation of the geosynthetic reinforced soil-integrated bridge system under static loading", *J. Geotech. Geoenviron. Eng.*, **143**(6), 04017008.  
[https://doi.org/10.1061/\(ASCE\)GT.1943-5606.0001665](https://doi.org/10.1061/(ASCE)GT.1943-5606.0001665).
- Zheng, Y., Fox, P.J., Shing, P.B. and McCartney, J.S. (2019), "Physical model tests of half-scale geosynthetic reinforced soil bridge abutments. I: Static loading", *J. Geotech. Geoenviron. Eng.*, **145**(11), 04019094.  
[https://doi.org/10.1061/\(ASCE\)GT.1943-5606.0002152](https://doi.org/10.1061/(ASCE)GT.1943-5606.0002152).
- Zheng, Y., McCartney, J.S. and Fox, P.J. (2018), "Numerical study on maximum reinforcement tensile forces in geosynthetic reinforced soil bridge abutments", *Geotext. Geomembr.*, **46**(5), 634-645. <https://doi.org/10.1016/j.geotexmem.2018.04.007>.

CC